Graphene Nanoribbon Composites

Mohammad A. Rafiee,[†] Wei Lu,[‡] Abhay V. Thomas,[†] Ardavan Zandiatashbar,[†] Javad Rafiee,[†] James M. Tour,[‡,*] and Nikhil A. Koratkar[†,*]

[†]Department of Mechanical, Aerospace and Nuclear Engineering, Rensselaer Polytechnic Institute, Troy, New York, 12180, United States, and [‡]Departments of Chemistry and Mechanical Engineering and Materials Science and the Smalley Institute for Nanoscale Science and Technology, Rice University, MS 222, Houston, Texas 77005, United States

ARTICLE

ABSTRACT It is well established that pristine multiwalled carbon nanotubes offer poor structural reinforcement in epoxy-based composites. There are several reasons for this which include reduced interfacial contact area since the outermost nanotube shields the internal tubes from the matrix, poor wetting and interfacial adhesion with the heavily cross-linked epoxy chains, and intertube slip within the concentric nanotube cylinders leading to a sword-in-sheath type failure. Here we demonstrate that unzipping such multiwalled carbon nanotubes into graphene nanoribbons results in a significant improvement in load transfer effectiveness. For example, at ~0.3% weight fraction of nanofillers, the Young's modulus of the epoxy composite with graphene nanoribbons shows ~30% increase compared to its multiwalled carbon nanotube counterpart. Similarly the ultimate tensile strength for graphene nanoribbons at ~0.3% weight fraction showed ~22% improvement compared to multiwalled carbon nanotubes at the same weight fraction of nanofillers in the composite. These results demonstrate that unzipping multiwalled carbon nanotubes into graphene nanoribbons can enable their utilization as high-performance additives for mechanical properties enhancement in composites that rival the properties of singlewalled carbon nanotube composites yet at an order of magnitude lower cost.

KEYWORDS: graphene nanoribbons · multiwalled carbon nanotubes · nanocomposites · mechanical properties · structural reinforcement

Graphene nanoribbons (GNRs), thin elongated strips of sp^2 bonded carbon atoms, can be fabricated by unzipping carbon nanotubes (CNTs).[1−3] The outstanding electronic and spin transport properties of GNRs make them attractive materials in a wide range of device applications.[3−5] GNRs have been produced by several techniques including lithographic,[6,7] chemical,[8] sonochemical,[3] and chemical vapor deposition (CVD).[9] Recently, Dai and co-workers have synthesized microscopic quantities of narrow nanoribbons by unzipping CNTs using the plasma etching route in the gas-phase.[2] In the present study, we applied the solution-based oxidative method,[1,10] synthesizing bulk quantities of thermally treated GNRs, for epoxy nanocomposite applications.

While two-dimensional graphene sheets derived from graphite oxide and other graphite intercalation compounds have been extensively used for structural reinforcement in composites, to the best of our knowledge this is the first report on the mechanical properties of GNR−polymer composites. Herein we investigated the tensile strength, Young's modulus, ductility, and toughness of an epoxy polymer reinforced with thermally treated GNRs. The results were compared to those of multiwalled carbon nanotube (MWNT) epoxy composites to establish the effect of the unzipping role of the MWNTs on the mechanical properties of the composite. We also compared the theoretically predicted elastic properties (using the Halpin−Tsai model) of GNR composites with our experimental data. The comparison reveals that the dispersion quality of GNR appears to have degraded above ~0.3% GNR weight fraction. The model predictions indicate that further improvements in the mechanical properties are possible if the dispersion of GNRs in the epoxy matrix can be improved at the higher nanofiller loading fractions.

MWNTs were unzipped based on a solution-based oxidative mechanism by engaging permanganate in an acid. A chemical reduction step was then used to relieve oxygen containing bonds resulting in graphene oxide nanoribbon (GONR) strips.[1] The synthesized GONRs were thermally reduced (heated to ~1050 °C in ~35 s) to expel oxygen groups and create GNRs. The protocols employed to thermally treat the GONRs are provided in the Materials and Methods section. The as-produced GNRs were dispersed in a bisphenol A based thermosetting epoxy by ultrasonication and high-speed mixing (Materials and Methods). Additional details regarding our dispersion method are available in refs 11−14. To investigate the mechanical properties of the nanocomposite, uniaxial (static) tensile

*Address correspondence to tour@rice.edu, koratn@rpi.edu.

Received for review September 24, 2010 and accepted November 09, 2010.

Published online November 16, 2010. 10.1021/nn102529n

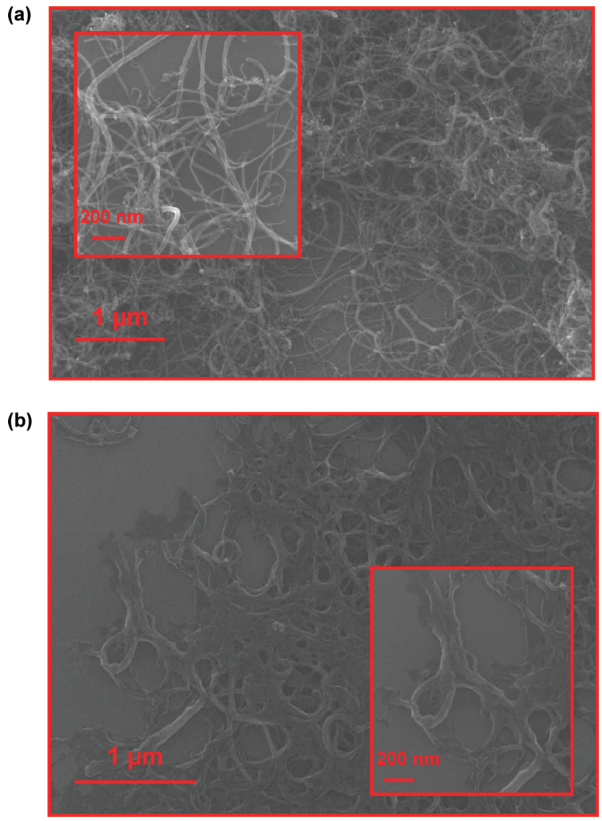

Figure 1. Scanning electron microscopy (SEM) characterization of the multiwalled carbon nanotubes (a) before and (b) after the oxidation process. Complete unzipping of the multiwalled carbon nanotubes into graphene oxide nanoribbons is evident from the images. As-produced graphene oxide nanoribbons were subsequently thermally reduced to yield graphene nanoribbons.

tests were conducted on dog-bone-shaped coupons. The Young's modulus of the nanocomposites were determined and compared to the predictions of the well-established Halpin−Tsai model for fiber-reinforced composite materials. In addition, we also characterized the ultimate tensile strength, ductility, and the toughness of the GNR/epoxy and MWNT/epoxy composites in comparison to the baseline (pristine) epoxy.

Figure 1a,b depicts scanning electron microscopy (SEM) images of MWNTs before and after the oxidation process. The purified MWNTs were procured from Bayer Corporation's Baytubes, and have an average outer diameter of ~14 nm, inner diameter of ~10 nm, and length in the range of 1−10 μm. As seen in the SEM images, MWNTs were completely unzipped, resulting in complex, wavy-structured GONRs strips. The typical width of the strips lies in the 50−100 nm range, while the length of the strips lies in the 1−10 μm range. Our simple solution-based oxidative process[1] generates a nearly 100% yield of nanoribbon structures by lengthwise cutting and unravelling of the MWNT side walls. Oxygen groups in the GONR were later eliminated by thermal reduction (Materials and Methods section). The GNR were uniformly dispersed by ultrasonication and high-speed shear mixing (Materials and Methods section) in the epoxy resin and cured to generate dog-bone-shaped coupons for the uniaxial tensile characterization. The weight fraction of GNR additives was varied in the 0−0.4% range. Figure 2a depicts a typical scanning electron micrograph of the freeze-fractured surface of the GNR/epoxy nanocomposite for ~0.3% weight fraction of GNR. The image shows GNR additives dispersed in the matrix; there was no indication of a large agglomeration or clustering of the fillers. Moreover the GNRs do not pull-out easily from the fracture surface as is typical of MWNTs. The inset in Figure 2a depicts a zoom-in SEM image of a GNR cluster that does appear to have been pulled out of the matrix. A

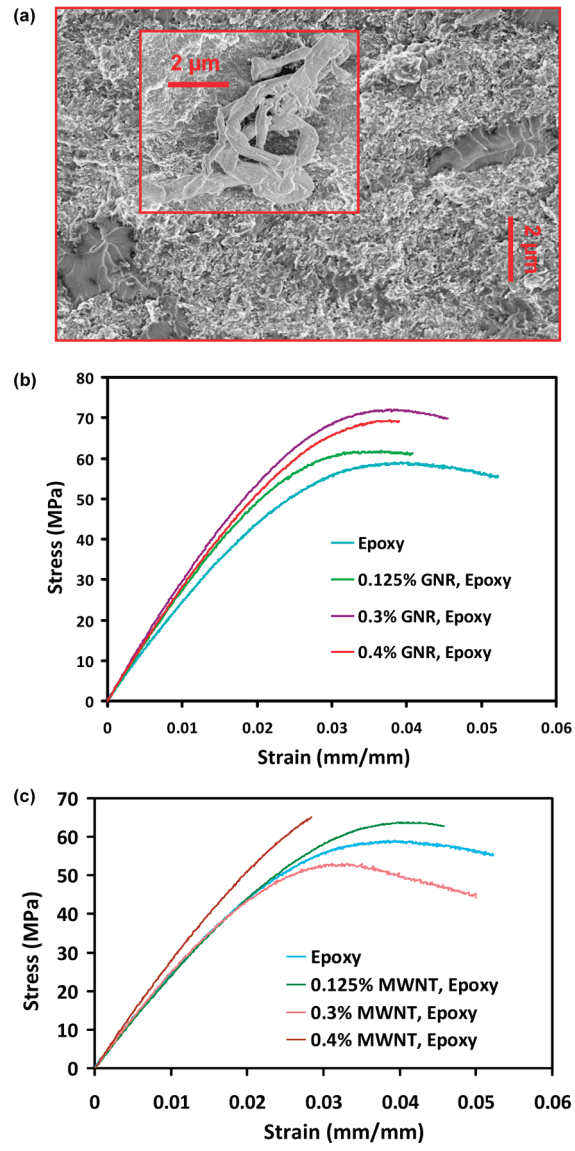

Figure 2. (a) Typical SEM image of free-fractured surface of graphene nanoribbon epoxy composite with ~0.3% weight of nanofillers. Inset shows a high resolution image of an agglomerated nanoribbon cluster surrounded by the matrix-rich region. (b) Typical stress *vs* strain curve of the baseline epoxy and nanocomposite formulations with varying weight fractions of graphene nanoribbon additives. (c) Corresponding stress *vs* strain response for MWNT/epoxy composites.

low number density of such pulled out clusters was observed on the fracture surface of the composite. For the most part the epoxy polymer appears to wet the GNR surface, which suggests a strong interface. Note that MWNTs suffer from intertube slip which degrades their ability as structural reinforcement additives. While interlayer slip is not completely overcome in GNR, there is a larger surface area on the GNRs available for interaction with the host epoxy.

Uniaxial tensile tests were conducted at a crosshead speed of ~1.5 mm/min at room temperature (~23 °C) using an MTS-858 system operated in the displacement control mode. Details regarding the sample geometry used for tensile testing are provided in the Supporting Information. Figure 2b illustrates the typical stress−strain response of the baseline epoxy and GNR/epoxy composites for ~0.125%, ~0.3%, and ~0.4% weight fraction of GNR additives. The GNR composites exhibit significant increase in the Young's modulus and the ultimate tensile strength compared to the baseline epoxy at the expense of a drop in the ductility (*i.e.*, the strain-to-break). The tests were also repeated for MWNT/epoxy composites at the same nanofiller loading fractions (Figure 2c). To check for statistics, between three to five specimens at each nanofiller weight fraction were tested, and the ultimate tensile strength (UTS) and Young's moduli (*E*) were determined (Figure 3a,b). The tensile strength of MWNT composites only increased by ~2−4% compared to the pristine epoxy, while the tensile strength of the ~0.3% weight GNR/epoxy nanocomposite increased by ~22%. There was no significant increase in the Young's modulus of the MWNT/epoxy composites, confirming that pristine MWNTs are poor additives for reinforcing highly cross-linked epoxy polymers which are unable to wrap around and interlock effectively with the atomistically smooth carbon nanotube surfaces.[15] By contrast, for ~0.3% weight of GNR additives, the Young's modulus showed over 30% increase compared to the baseline epoxy and the MWNT-reinforced epoxy. Considering that our tests were performed on a heavily cross-linked epoxy (which displays an inherently high level of modulus/strength), this is an impressive level of increase in mechanical properties at low nanofiller loading. By comparison, for ~1% weight of functionalized singlewalled carbon nanotube (SWNT) fillers in epoxy, Zhu *et al.* reported ~30% and ~15% increases in the

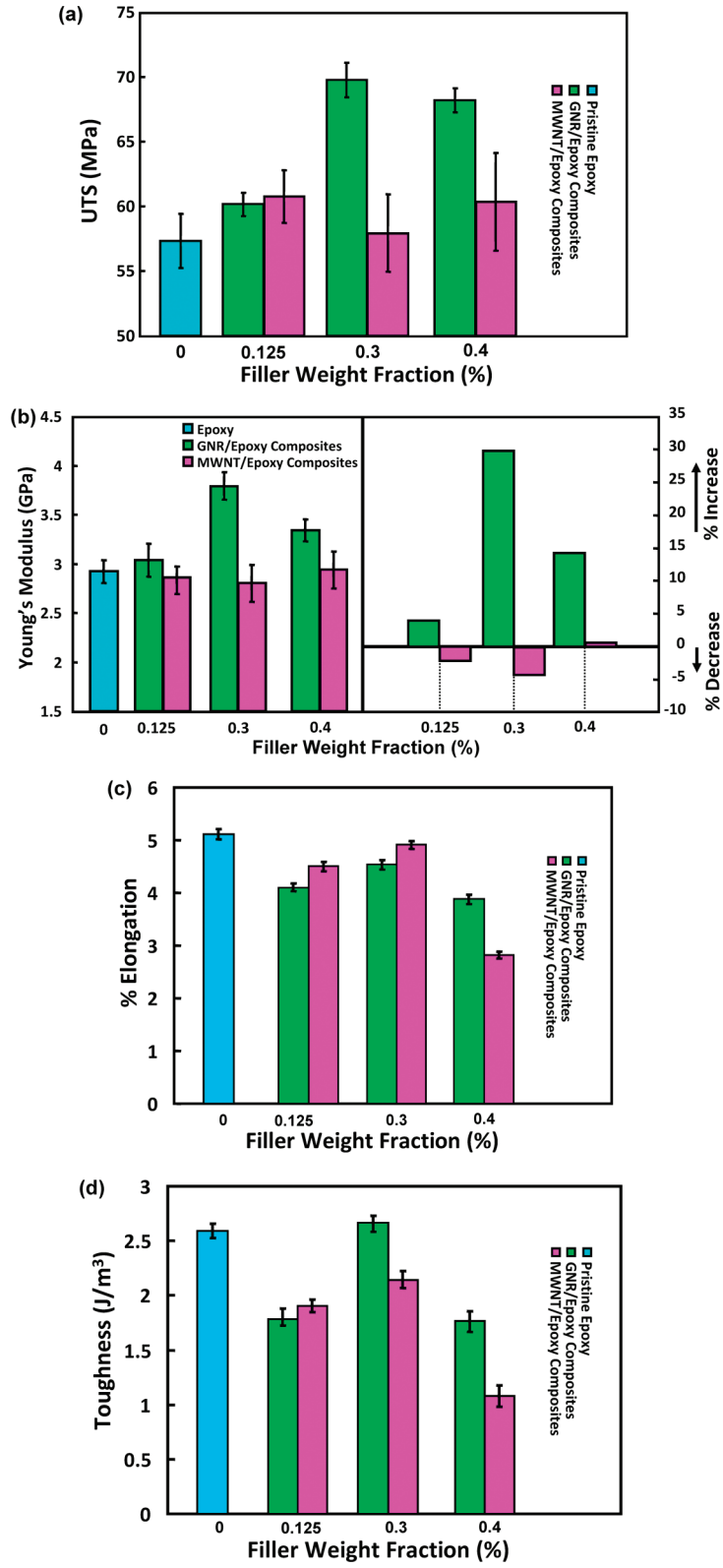

Figure 3. Uniaxial mode tensile testing. (a) Averaged results for the ultimate tensile strength (UTS) for the baseline epoxy and nanocomposites with varying loading fraction of nanofillers. (b) Absolute value and percentage changes in the Young's modulus of the pristine epoxy and nanocomposites with various nanofiller weight fractions. (c) Percent elongation at failure for the baseline epoxy and nanocomposites with various nanofiller weight fractions. (d) Corresponding results for the material toughness (*i.e.*, the total area under the stress *vs* strain curves) for the baseline epoxy and the various nanocomposite formulations.

Young's modulus and the tensile strength, respectively.[16] In our case, we demonstrate similar levels of enhancement in the modulus and strength for GNR composites at ~70% lower weight fraction of the nanofillers.

In addition to tensile strength and modulus, we also compared the ductility (*i.e.*, strain-to-break) and the toughness (*i.e.*, energy absorbed at failure which is the total area under the stress *vs* strain curve) of the baseline and nanocomposite epoxies. Figure 3c indicates that the ductility of the GNR composites is about 10−15% lower than the pristine epoxy. The reduced ductility may be caused by stress concentration in the vicinity of the filler; this typically occurs when hard fillers are incorporated into a brittle matrix. Besides, agglomeration of GNR can lead to defects in the matrix that can act as seed points for crack initiation and premature fracture. Similar loss of ductility was also seen for MWNT composites (Figure 2c and Figure 3c). Ductility is usually critical for metals where the manufacturing processes are based on metal forming operations (*e.g.*, rolling, extrusion). For epoxies, 10−15% loss in ductility can be tolerated provided that other mechanical properties such as modulus and strength are enhanced. Figure 3d shows the material toughness for the baseline epoxy and the MWNT and GNR epoxy nanocomposites. MWNT composites show lower toughness than the baseline epoxy, while for the ~0.3% weight fraction GNR/epoxy composite the toughness is marginally increased compared to the baseline epoxy.

To predict the elastic properties of the GNR/epoxy composites, the GNR strips were modeled as rectangular cross-section fibers having width (W), length (L), and thickness (t). The well-established Halpin−Tsai equations[17−19] developed for randomly oriented fiber reinforcement were applied as follows:

$$\alpha = \frac{E_C}{E_M} = \frac{3}{8}\left(\frac{\zeta\eta_L V_{GNR} + 1}{1 - \zeta\eta_L V_{GNR}}\right) + \frac{5}{8}\left(\frac{2\zeta\eta_W V_{GNR} + 1}{1 - \zeta\eta_W V_{GNR}}\right) \quad (1)$$

$$\eta_L = \frac{\beta - 1}{\beta + \zeta} \quad (2)$$

$$\eta_W = \frac{\beta - 1}{\beta + 2} \quad (3)$$

where α is the ratio of the composite's modulus (E_C) to that of the pure epoxy (E_M), $E_{GNR} = 1$ TPa is the Young's modulus of GNRs, V_{GNR} is the GNR volume fraction, and ζ and β are constants which are defined as follows:

$$\zeta = \frac{W + L}{t} \quad (4)$$

$$\beta = \frac{E_{GNR}}{E_M} \quad (5)$$

Substituting from equations 2−5 into eq 1, the ratio of the composite's modulus (E_C) to that of the pure epoxy (E_M) can be expressed as a function of the volume fraction of reinforcements as follows:

$$\alpha = \frac{E_C}{E_M} = \frac{3}{8}\left(\frac{((W + L)/t)\dfrac{(E_{GNR}/E_M) - 1}{(E_{GNR}/E_M) + ((W + L)/t)}V_{GNR} + 1}{1 - \dfrac{(E_{GNR}/E_M) - 1}{(E_{GNR}/E_M) + ((W + L)/t)}V_{GNR}}\right) + \frac{5}{8}\left(\frac{2\dfrac{(E_{GNR}/E_M) - 1}{(E_{GNR}/E_M) + 2}V_{GNR} + 1}{1 - \dfrac{(E_{GNR}/E_M) - 1}{(E_{GNR}/E_M) + 2}V_{GNR}}\right) \quad (6)$$

The weight fraction of GNRs was converted into volume fraction based on the estimated densities of GNRs and the epoxy. On the basis of information provided by the MWNT supplier and our SEM characterization, the average size of GNRs was estimated as ~5 μm in length (L), ~78 nm in width (W), and ~4 nm in thickness (t). As a conservative estimate, the density of the GNRs was taken as the standard density of graphite (~2.25 g/cm^3). Figure 4 shows the results of the theoretical predictions from eq 6 in comparison to the experimental values. There is reasonable agreement between theory and experiment until ~0.13% volume fraction (*i.e.*, 0.3% weight fraction), beyond which the experimental data for the Young's modulus begins to drop off below the theoretical prediction. This suggests that the quality of dispersion of GNR in the epoxy resin begins to degrade beyond a weight fraction of ~0.3%. This result is consistent with two-dimensional graphene platelets which begin to agglomerate at even lower weight fractions (~0.1%) in epoxy matrices.[11] This highlights the need for continued research to develop new methods to enhance GNR dispersion at higher loading fractions in order to derive the full benefit of these unique materials for structural composites.

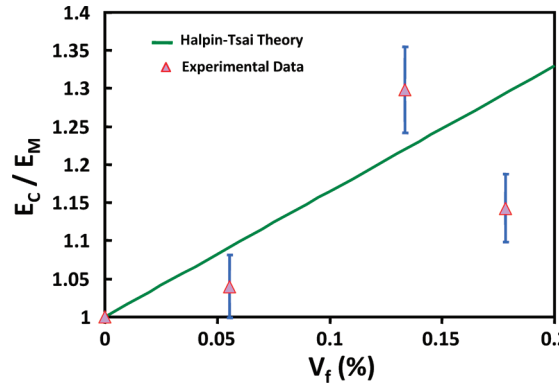

Figure 4. Theoretical predictions from the Halpin−Tsai model for normalized Young's modulus of graphene nanoribbon composites plotted *versus* nanofiller volume fraction, indicating reasonable agreement between theory and experimental data up to ~0.13% volume fraction (~0.3% weight fraction) of nanofillers.

To understand the underlying mechanisms that are responsible for the improved performance of GNR, we compared the surface chemistry and defect density of MWNTs, GONRs, and GNRs using X-ray photoelectron spectroscopy (XPS) and Raman spectroscopy. We find that the surface chemistry of the MWNTs and GNRs used in the testing is very similar as confirmed by XPS characterization (Supporting Information). The elimination of oxygen containing groups was confirmed by the C1s spectrum of GNR (Supporting Information), since no peaks corresponding to C−O (~286 eV) and C═O (~287.8 eV)[10,20,21] bonds were observed for the thermally reduced GNRs. Consequently, surface chemistry alone is not responsible for enhanced effectiveness of GNRs over MWNTs as a structural reinforcement additive. The Raman spectra for GNRs and MWNTs (Supporting Information) indicate that the ratio of the integrated intensity of the D band to G band is ~1.25 for GNR compared to ~1.04 for MWNT indicating that the GNRs are somewhat more defective than MWNTs, and likely provide greater handles for interaction with the host epoxy. More importantly, however, is the surface area of the nanoribbons relative to the tubular structures; therefore, taken together, the nanoribbons are superior. The average specific surface area of the MWNT and GNR samples in the powder form was measured by standard BET N_2 cryosorption experiments (see Supporting Information). The specific surface area of GNR (~511 m^2/g) was found to be significantly greater than that of a MWNT (~291 m^2/g). This confirms that the combined GNR surface areas are far greater than that of the MWNTs from which they are derived, and this likely contributes considerably to the strong interfacial interaction of the GNRs in epoxy rather than MWNT interactions in epoxies at the same weight loadings.

CONCLUSION

While pristine MWNTs are ineffective at reinforcing epoxy composites, unzipping them into GNRs results in significant improvement. In our view, the two main factors responsible for this are as follows. (1) Surface area: The unraveling of MWNT into GNR platelets generates a significant increase in the interfacial contact area since both surfaces of each individual GNR platelet will contact the matrix, as opposed to only the outermost cylinder of the MWNT. (2) Geometry: It is challenging for highly cross-linked polymers such as epoxies to wrap around tubular MWNTs (with 10−20 nm diameter) and mechanically interlock with them. We expect that it is easier for such polymers to adhere to a flat nanofiller with a sheet or ribbonlike geometry. The GNRs are also more defective than MWNTs, which contributes to better interfacial binding. These results indicate that GNRs show significant potential as a structural reinforcement additive in polymer-based composite materials.

MATERIALS AND METHODS

GNR Preparation. A mixture of sulfuric acid (98%, 180 mL) and phosphoric acid (85.8%, 20 mL) was added to Baytubes (lot no. C70P, 1 g, 83 mmol), and the mixture was stirred. Potassium permanganate (6 g, 38 mmol) was added in three portions over ~30 min to the reaction mixture. After ~15 min, the mixture was heated to ~45 °C and stirred at that temperature for ~24 h. The reaction mixture was cooled to room temperature and poured onto ice containing ~10 mL of hydrogen peroxide (30%). The GONRs were collected by centrifuging the mixture at 4100 rpm for ~90 min. After the solution was decanted, the resulting wet GONRs were redispersed in ~150 mL of hydrochloric acid (10%) and centrifuged again. This process was repeated two more times. Then the wet GONRs were dispersed in ~50 mL DI water and transferred to a dialysis bag and dialyzed in running DI water for 1 week to remove the residual acid and inorganic salts. The water was removed under reduced pressure, and the GONRs were dried in a vacuum oven at ~70 °C for ~16 h. Finally, the as-produced GONRs were thermally reduced to GNRs by insertion for ~35 s into a tube furnace (Thermolyne 79300, Thermo Fisher Scientific, Inc., USA) preheated to ~1050 °C.

Nanocomposite Processing. GNRs were first dispersed in acetone (~200 mL of acetone per ~0.1 g of GNR) by high amplitude ultrasonication (Sonics Vibracell VC 750, Sonics and Materials Inc., USA) for ~1.5 h in an ice bath. A thermo-setting epoxy resin (Epoxy-2000 from Fibreglast Inc., USA) was added to the solution and sonicated, following the same procedure. The acetone was removed through heating and magnet stirring the mixture for ~3 h at ~70 °C. To eliminate any trace amount of acetone remaining, the mixture was placed into a temperature controlled vacuum chamber for ~12 h (at ~70 °C). After, the GNR/epoxy blend cooled down to room temperature, a curing agent (2120 from Fibreglast Inc., USA) was added and mixed by using a high speed shear mixer (ARE-250, Thinky, Japan) at ~2000 rpm (for ~4 min). Finally, the mixture is degassed for ~30 min in a vacuum chamber and is poured into silicon molds for curing under ~90 psi pressure (for 24 h) and postcuring at ~90 °C (for 4 h). The same procedure was followed for dispersion of MWNTs in the epoxy matrix.

Acknowledgment. N.A.K. acknowledges funding support from the USA Office of Naval Research (Award Number: N000140910928) and the USA National Science Foundation (Award Number: 0900188). J.M.T. thanks Dr. Horst Adams of Bayer Corp. for graciously providing the MWNTs and the Federal Aviation Administration (2007G010) and Air Force Office of Scientific Research (FA9550-09-1-0581) for financial support.

Supporting Information Available: BET surface area analysis, XPS characterization, Raman spectroscopy characterization, dispersion of GNR and GONR in acetone, sample geometry, and dimensions for uniaxial tensile mode testing. This material is available free of charge *via* the Internet at http://pubs.acs.org.

REFERENCES AND NOTES

1. Higginbotham, A. L.; Kosynkin, D. V.; Sinitskii, A.; Sun, Z.; Tour, J. M. Low-Defect Graphene Oxide Nanoribbons from Multiwalled Carbon Nanotubes, *ACS Nano* **2010**, *4*, 2059–2069.
2. Jiao, L.; Zhang, L.; Wang, X.; Diankov, G.; Dai, H. Narrow Graphene Nanoribbons from Carbon Nanotubes. *Nature* **2009**, *458*, 877–880.
3. Kosynkin, D. V.; Higginbotham, A. L.; Sinitskii, A.; Lomeda, J. R.; Dimiev, A.; Price, B. K.; Tour, J. M. Longitudinal Unzipping of Carbon Nanotubes To Form Graphene Nanoribbons. *Nature* **2009**, *458*, 872–876.

4. Li, X.; Wang, X.; Zhang, L.; Lee, S.; Dai, H. Chemically Derived, Ultrasmooth Graphene Nanoribbon Semiconductors. *Science* **2008**, *319*, 1229–1232.
5. Wang, X.; Li, X.; Zhang, L.; Yoon, Y.; Weber, P. K.; Wang, H.; Guo, J.; Dai, H. *N*-Doping of Graphene through Electrothermal Reactions with Ammonia. *Science* **2009**, *324*, 768–771.
6. Han, M. Y.; Oezyilmaz, B.; Zhang, Y.; Kim, P. Energy Band-Gap Engineering of Graphene Nanoribbons. *Phys. Rev. Lett.* **2007**, *98*, 206805.
7. Chen, Z.; Lin, Y.-M.; Rooks, M. J.; Avouris, P. Graphene Nanoribbon Electronics. *Phys. E* **2007**, *40*, 228–232.
8. Schniepp, H. C.; Li, J. -L.; McAllister, M. J.; Sai, H.; Herrera-Alonso, M.; Adamson, D. H.; Prud'homme, R. K.; Car, R.; Saville, D. A.; Aksay, I. A. Functionalized Single Graphene Sheets Derived from Splitting Graphite Oxide. *J. Phys. Chem. B* **2006**, *110*, 8535–8539.
9. Campos-Delgado, J.; Romo-Herrera, J. M.; Jia, X.; Cullen, D. A.; Muramatsu, H.; Kim, Y. A.; Hayashi, T.; Ren, Z.; Smith, D. J.; Okuno, Y.; *et al*. Bulk Production of a New Form of sp^2 Carbon: Crystalline Graphene Nanoribbons. *Nano Lett.* **2008**, *8*, 2773–2778.
10. Marcano, D. C.; Kosynkin, D. V.; Berlin, J. M.; Sinitskii, A.; Sun, Z.; Slesarev, A.; Alemany, L. B.; Lu, W.; Tour, J. M. Improved Synthesis of Graphene Oxide. *ACS Nano* **2010**, *4*, 4806–4814.
11. Rafiee, M. A.; Rafiee, J.; Srivastava, I.; Wang, Z.; Song, H.; Yu, Z.-Z.; Koratkar, N. Fracture and Fatigue of Graphene Nanocomposites. *Small* **2010**, *6*, 179–183.
12. Rafiee, M. A.; Rafiee, J.; Yu, Z.-Z.; Koratkar, N. Buckling Resistant Graphene Nanocomposites. *Appl. Phys. Lett.* **2009**, *95*, 223103.
13. Rafiee, M. A.; Rafiee, J.; Wang, Z.; Song, H.; Yu, Z.-Z.; Koratkar, N. Enhanced Mechanical Properties of Nanocomposites at Low Graphene Content. *ACS Nano* **2009**, *3*, 3884–3890.
14. Rafiee, M. A.; Rafiee, J.; Z-Z; Yu, N. Koratkar, Superhydrophobic to Superhydrophilic Wetting Control in Graphene Films. *Adv. Mater.* **2010**, *22*, 2151–2154.
15. Suhr, J.; Koratkar, N.; Keblinski, P.; Ajayan, P. M. Viscoelasticity in Carbon Nanotube Composites. *Nat. Mater.* **2005**, *4*, 134–137.
16. Zhu, J.; Kim, J.; Peng, H.; Margrave, J. L.; Khabashesku, V. N.; Barrera, E. V. Improving the Dispersion and Integration of Single-Walled Carbon Nanotubes in Epoxy Composites through Functionalization. *Nano Lett.* **2003**, *3*, 1107–1113.
17. Mallick, P. K. *Fiber-Reinforced Composites*; Dekker: New York, 1993; p 130.
18. Thostenson, E. T.; Chou, T.-W. On the Elastic Properties of Carbon Nanotube-Based Composites: Modelling and Characterization. *J. Phys. D: Appl. Phys.* **2003**, *36*, 573–582.
19. Halpin, J. C.; Tsai, S. W. Environmental Factors in Composite Materials Design. *U.S. Air Force Tech. Rep. AFML TR* **1967**, 67–423.
20. Stankovich, S.; Dikin, D. A.; Dommett, D.; Kohlhaas, K.; Zimney, E. J.; Stach, E. A.; Piner, R. D.; Nguyen, S. T.; Ruoff, R. S. Graphene-Based Composite Materials. *Nature* **2006**, *442*, 282–285.
21. Ramanathan, T.; Abdala, A. A.; Stankovich, S.; Dikin, D. A.; Herrera-Alonso, M.; Piner, R. D.; Adamson, D. H.; Schniepp, H. C.; Chen, X.; Ruoff, R. S.; *et al*. Functionalized Graphene Sheets for Polymer Nanocomposites. *Nat. Nanotechnol.* **2008**, *3*, 327–331.